Journal of Biomedical Optics

SPIEDigitalLibrary.org/jbo

Wide-field optical sectioning for live-tissue imaging by plane-projection multiphoton microscopy

Jiun-Yann Yu
Chun-Hung Kuo
Daniel B. Holland
Yenyu Chen
Mingxing Ouyang
Geoffrey A. Blake
Ruben Zadoyan
Chin-Lin Guo

SPIE

Wide-field optical sectioning for live-tissue imaging by plane-projection multiphoton microscopy

Jiun-Yann Yu,[a] Chun-Hung Kuo,[b] Daniel B. Holland,[c] Yenyu Chen,[d] Mingxing Ouyang,[a] Geoffrey A. Blake,[c,e] Ruben Zadoyan,[b] and Chin-Lin Guo[a]

[a]California Institute of Technology, Bioengineering, 1200 E. California Boulevard, MC 138-78, Pasadena, California 91125
[b]Newport Corporation, Technology and Applications Center, 1791 Deere Avenue, Irvine, California 92606
[c]California Institute of Technology, Division of Chemistry and Chemical Engineering, 1200 E. California Boulevard, MC 139-74, Pasadena, California 91125
[d]Stanford University, Center for Cardiovascular Technology, 300 Pasteur Drive, Palo Alto, California 94305
[e]California Insitute of Technology, Division of Geological and Planetary Sciences, 1200 E. California Boulevard, MC 150-21, Pasadena, California 91125

Abstract. Optical sectioning provides three-dimensional (3D) information in biological tissues. However, most imaging techniques implemented with optical sectioning are either slow or deleterious to live tissues. Here, we present a simple design for wide-field multiphoton microscopy, which provides optical sectioning at a reasonable frame rate and with a biocompatible laser dosage. The underlying mechanism of optical sectioning is diffuser-based temporal focusing. Axial resolution comparable to confocal microscopy is theoretically derived and experimentally demonstrated. To achieve a reasonable frame rate without increasing the laser power, a low-repetition-rate ultrafast laser amplifier was used in our setup. A frame rate comparable to that of epifluorescence microscopy was demonstrated in the 3D imaging of fluorescent protein expressed in live epithelial cell clusters. In this report, our design displays the potential to be widely used for video-rate live-tissue and embryo imaging with axial resolution comparable to laser scanning microscopy. [DOI: 10.1117/1.3647570]

Keywords: microscopy; multiphoton processes; diffusers; imaging systems.

Paper 11137RR received Mar. 22, 2011; revised manuscript received Sep. 3, 2011; accepted for publication Sep. 19, 2011; published online Nov. 3, 2011.

1 Introduction

Optical sectioning and high-acquisition-rate imaging techniques have been established for decades, but very few techniques have been proposed to provide optical sectioning at a reasonable frame rate and with a biocompatible laser dosage for live-tissue imaging. Most optical-sectioning techniques rely on a scanned optical probe point.[1] However, to obtain images at a reasonable frame rate, the excitation intensity of laser scanning microscopy often has to be significantly stronger than wide-field microscopy; this is due to the extremely short dwell time per pixel in laser scanning microscopy. Consequently, for confocal microscopy, significant phototoxicity can occur in scanned live organisms if a video-rate time-lapse microscopy is required.[1] Such phototoxicity can be greatly reduced by using multiphoton microscopy,[2,3] but a tradeoff is the thermal mechanical damage to live tissue through the single-photon absorption of the near-infrared excitation.[4]

One potential way to resolve photo/thermal-damage in scanning microscopy without the loss of acquisition speed is to implement the capability of optical sectioning in wide-field microscopy. Several methods have been proposed to fulfill this goal.[5–9] These methods can be categorized into two main regimes: single-photon excitation and multiphoton excitation.

In wide-field single-photon excitation, the most well-known methods include light-sheet illumination microscopy and structured light microscopy.[5,6] Both methods are technically elaborate, introducing complexity into the optical system due to the requirement of additional mechanical parts that synchronize with axial scanning components. Moreover, light-sheet microscopy obtains optical sectioning by illuminating the sample laterally (i.e., perpendicular to the optical axis); this introduces significant mechanical complexity and makes the preparation of samples difficult. Furthermore, structured light microscopy excites the full sample volume and requires multiple exposures for each single position—an extremely inefficient use of the quantum yield of the fluorophores.[6]

For wide-field multiphoton excitation, a key element to maintain the capability of optical sectioning is to create significant time delays among positions excited in the illumination field,[7,8] as we discuss in Sec. 2. Consequently, the complexity of the systems is further increased by the need to engineer sufficient time delays, and the number of pixels has been very limited (<100).[7,8]

The concept of time delays in wide-field multiphoton excitation was later generalized into an optical design referred to as temporal focusing.[9] In a temporal focusing setup, the pulse width of the excitation light varies in time as the pulse propagates along the optical axis, and is shortest at the image plane (Fig. 1 inset); the higher peak intensity associated with a shorter pulse width provides the optical sectioning effect.

Address all correspondence to: Jiun-Yann Yu, California Institute of Technology, 1200 E California Blvd, MC 138-78, Pasadena, CA 91125; Tel: 626-395-5992; E-mail: jyyu@caltech.edu.

1083-3668/2011/16(11)/116009/9/$25.00

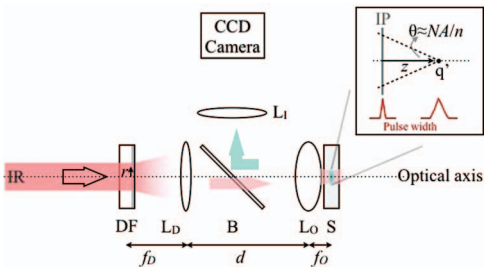

Fig. 1 The setup of a plane-projection multiphoton microscope. The ultrafast infrared laser beam (IR, red) from the left is scattered by a diffuser (DF). The image of the surface of DF is then projected to the sample to excite a thin plane (green). The zoomed-in inset shows that light arriving at an out-ot-focus point q' is mainly from points within a cone angle θ on the image plane, and that the different arrival times elongate the effective pulse width at q'. L_D: diffuser lens of focal length f_D. B: beamsplitter. L_O: microscope objective of focal length f_O. S: sample; L_I: imaging lens. IP: image plane.

Temporal focusing for microscopy was first experimentally demonstrated by Oron et al.[9] In their setup, the laser pulse is directed to a blazed grating (which serves as a scatterer) in an oblique incidence orientation. This creates a line-scan mechanism, which leads to the time delay across the image plane, thereby generating optical sectioning.[9] There exist two issues, however, in this technique. First and primarily, a unique blazed diffraction grating must be fabricated for each specific wavelength window. Exciting multiple fluorophores, as is required for most biomedical studies, would require multiple gratings and hence increases the complexity of the system. Second, the signal level obtained by the previous temporal focusing setup[9] is weaker by several orders of magnitude than that which can be achieved by conventional scanning microscopy. The low signal level results from the dilution of the excitation intensity in a wide-field setup. Consequently, the image acquisition rate is significantly reduced. For example, in Oron et al.'s original report,[9] the frame rate is roughly 0.033 frames per second (fps) for cells stained with DAPI (a fluorescent dye for chromosome staining), which is much brighter than most biological fluorophores expressed in live tissues.

Here, we present a simple approach to remove the limitations associated with a single excitation wavelength and low acquisition rates in temporal-focusing microscopes. One way to overcome the limitation of single wavelength excitation is to use an optical diffuser rather than a blazed grating as the scatterer, because the scattering pattern of an optical diffuser is insensitive to the central wavelength of the excitation light. A theoretical estimation by Oron et al., however, suggests that using optical diffusers to create temporal focusing requires the pulse width of the laser to be shorter than 10 fs, even with high numerical-aperture (NA) objectives.[9] This would make diffuser-based temporal focusing almost impractical, given the current pulse width of most commercially available light sources (~100 fs). In their estimations, though, the optical diffuser was considered as an ideally flat plane of points generating ultrafast pulses simultaneously. In practice, a ground-glass diffuser has a rough surface, which introduces random time delays among the scattering points. In other words, the optical diffuser creates a plane of point sources having a distribution of time delays with respect to each other, instead of zero time delay as was previously modeled. By projecting these point sources onto the sample plane of the microscope, temporal focusing, and hence optical sectioning, can be achieved. Therefore, we refer to our technique as "plane-projection multiphoton" (PPMP) microscopy. Through geometrical calculations, we found that using an optical diffuser should enable optical sectioning comparable to confocal microscopy, even with moderate NA objectives and pulse widths up to 100 fs.

For the other issue of temporal focusing, the low acquisition rate, one needs a way to increase the signal level. Recent studies suggest that using ultrafast laser amplifiers with a repetition rate of approximately a few hundred kilohertz might significantly enhance the signal level, without increasing the average power.[9] To examine this possibility, we theoretically derived the dependence of the multiphoton excitation upon the pulse repetition rate while the average power remained constant. Our calculations suggest that for a field of view comparable to conventional epifluorescence microscopy, a repetition rate of approximately 1 kHz or slower could yield sufficient signal at a reasonable frame rate and with a biocompatible laser dosage for live-cell imaging. We experimentally verified this prediction by using a 1-kHz ultrafast amplifier to obtain the optical sectioning of fluorescent protein expressed in live epithelial tissues at a frame rate of 5 fps, a frame rate similar to that used in a conventional epifluorescence microscope to obtain images on the same sample. Thus, by using optical diffusers having sufficient surface roughness, and laser sources of sufficiently low repetition rate and high pulse energy, we have demonstrated a simple system design for obtaining 3D live-tissue images at an axial resolution comparable to conventional confocal microscopy. Furthermore, signal levels, and thus frame rates, are comparable with conventional epifluorescence microscopy.

2 Theory

2.1 *Efficiency of Temporal Focusing Through an Optical Diffuser*

In this section we reinvestigate the temporal focusing effect through an optical diffuser. Specifically, we compute the variation of the pulse width along the optical axis based on geometrical optics. An axial resolution comparable to conventional confocal microscopy is derived.

Figure 1 depicts the schematic of a typical temporal focusing setup.[9] An optical diffuser (DF) was used to transform the incoming ultrafast laser beam into a plane of point sources. These point sources were then projected onto the image plane (IP) of an infinity-corrected microscope, through the diffuser lens (L_D) and the objective (L_O). The resulting fluorescence was imaged onto a CCD camera through an imaging lens (L_I).

As discussed by Oron et al., the elongation of pulse width at an out-of-focus point q' at a distance z away from the IP can be estimated through the maximal difference of pulse arrival times from the point sources within a cone of angle θ from the IP (Fig. 1 inset).[9] Here, θ can be determined by the divergence angle of L_O, $\theta \approx \mathrm{NA}/n$ (Fig. 1 inset).[9] To estimate the difference of pulse arrival times resulting from the geometry of the setup,

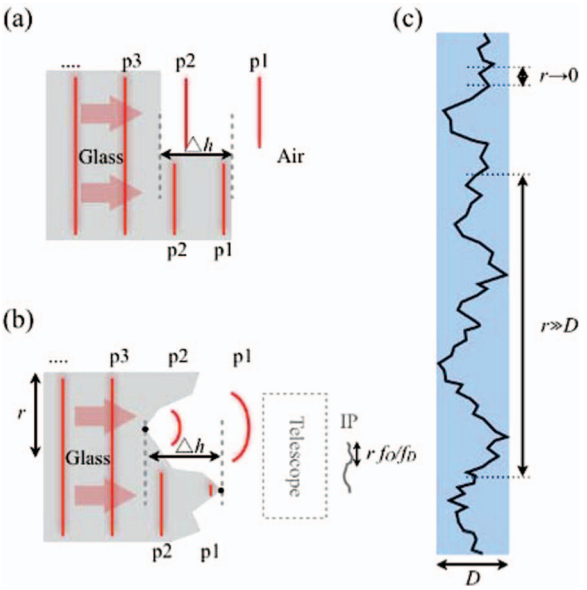

Fig. 2 Random time delay generated by the surface roughness of an optical diffuser. (a) The time delay of the laser pulses results from a discrepancy of height, Δh, on the diffuser surface. (b) A more general case for (a). Here, Δh corresponds to the maximal surface height discrepancy (i.e., the peak-to-valley difference) within an area of radius r (the corresponding area on the IP is of radius $r\,f_O/f_D$). (c) The schematic illustration of Δh under different scales of r. Upper: when $r \to 0$, $\Delta h \to 0$. Lower: when $r \gg D$, $\Delta h \approx D$.

we first considered the case where the DF is approximated as a flat plane of point sources that simultaneously generate ultrafast pulses. Using the lens formula and paraxial approximation, the elongation of the pulse width Δt_G at the point q' can be estimated as

$$\Delta t_G(z) \approx \frac{(f_D + f_O - d)\cdot \mathrm{NA}^2}{2\,C_0 \cdot n \cdot f_O^2}\cdot z^2 + n\,\frac{n - \sqrt{n^2 - \mathrm{NA}^2}}{C_0 \cdot \sqrt{n^2 - \mathrm{NA}^2}}\cdot z, \tag{1}$$

where C_0 is the speed of light in vacuum and n is the refractive index of the sample medium. The first term on the right-hand side arises from the difference of optical path lengths from the DF to IP, and the second term results from the difference of optical path lengths from IP to the point q'.

We next take into account the surface roughness of DF and estimate how such roughness leads to a randomness of arrival times. To proceed, we consider a simple case where the roughness is represented by a step function with a height discrepancy Δh on the diffuser surface [Fig. 2(a)]. The time delay of a pulse p1 induced by Δh is simply $\Delta h/C_{\mathrm{Glass}} - \Delta h/C_{\mathrm{Air}} = (n_{\mathrm{Glass}} - n_{\mathrm{Air}}) \cdot (\Delta h/C_0) \approx 0.5\,\Delta h\,/\,C_0$. Further, the time delay caused by the roughness in a region A_r of radius r on the diffuser surface is projected into a region A_r' of radius $r' = f_O\,/\,f_D\,r$ on the image plane [Fig. 2(b)]. The maximal time delay Δt_{RD} within $A_{r'}$ may thus be approximated as

$$\Delta t_{RD} = 0.5\,\frac{\Delta h}{C_0}, \tag{2}$$

where Δh is the maximal surface height discrepancy within A_r. In general, the roughness of a ground-glass diffuser is generated by grinding a flat surface of glass with particles of size less than a certain length D. Thus, we expect $\Delta h \to 0$ when $r \to 0$, and $\Delta h \approx D$ if $r \gg D$, as shown in Fig. 2(c). To take into account these asymptotic estimations, we used a simple approximation here: $\Delta h \approx \alpha \cdot 2r$ if $\alpha \cdot 2r < D$ and $\Delta h \approx D$ if $\alpha \cdot 2r \geq D$, where α is a dimensionless parameter describing the roughness of a diffuser. Using this approximation, we obtain a simple estimation of the difference of arrival times Δt_{RD} within $A_{r'}$,

$$\Delta t_{RD} = \begin{cases} \dfrac{\alpha\, f_D}{C_0 \cdot f_O}\cdot r' & \text{if } \dfrac{\alpha\, f_D}{f_O}\cdot r' < 0.5\,D \\ \dfrac{0.5\,D}{C_0} & \text{if } \dfrac{\alpha\, f_D}{f_O}\cdot r' \geq 0.5\,D \end{cases} = \frac{1}{C_0}\cdot \mathrm{Min}\left[\frac{\alpha\, f_D}{f_O}\,r',\ 0.5\,D\right]. \tag{3}$$

For the out-of-focus point q' shown in Fig. 1 (inset), $A_{r'}$ corresponds to the area covered by the cone angle θ, and so we have $r' \approx z \cdot \theta \approx \frac{\mathrm{NA}}{n} z$ and

$$\Delta t_{RD}(z) = \frac{1}{C_0}\cdot \mathrm{Min}\left[\frac{\alpha\, f_D}{f_O}\cdot\frac{\mathrm{NA}}{n}\cdot z\ ,\ 0.5\,D\right]. \tag{4}$$

Combining Eqs. (1) and (4), we finally obtain the effective pulse duration at an out-of-focus point q' at distance z from the IP, namely

$$\tau_{\mathrm{eff}}(z) = \tau_0 + \Delta t_{RD} + \Delta t_G \tag{5}$$

$$= \tau_0 + \frac{\mathrm{Min}\left[\frac{\alpha\, f_D}{f_O}\frac{\mathrm{NA}}{n} z\ ,\ 0.5\,D\right]}{C_0} + \frac{(f_D + f_O - d)\mathrm{NA}^2}{2\,C_0\,n\,f_O^2} z^2 + n\,\frac{n - \sqrt{n^2 - \mathrm{NA}^2}}{C_0\,\sqrt{n^2 - \mathrm{NA}^2}} z, \tag{6}$$

where τ_0 is the pulse width of the laser source.

Figure 3 shows the numerical results of $\tau_{\mathrm{eff}}(z)$ for the cases of three different sample objectives commonly used for biomedical microscopy. Consistent with a previous report,[9] we find that the contribution of Δt_G to $\tau_{\mathrm{eff}}(z)$ is negligible when z is within a few Rayleigh lengths (z_R). Nevertheless, in this small z regime, Δt_{RD}

in Eq. (6) can lead to a significant elongation of pulse width. In particular, for the small z regions where $\alpha f_D/f_O \cdot \mathrm{NA}/n \cdot z < 0.5D$, Eq. (6) can be simplified as

$$\tau_{\mathrm{eff}} \approx \tau_0 \left(1 + \frac{\alpha\, f_D}{f_O} \cdot \frac{\mathrm{NA}}{\tau_0\, n\, C_0} z\right) = \tau_0 \left(1 + \frac{\alpha\, f_D}{f_O} \cdot \frac{n\,\lambda}{\pi\, \tau_0\, C_0\, \mathrm{NA}} \bar{z}\right),$$

$$\text{with } \bar{z} \equiv \frac{z}{z_R} \approx \frac{\pi\, \mathrm{NA}^2}{n^2\,\lambda} z. \tag{7}$$

Here, $\bar{z}$ is defined in units of Rayleigh length in order to facilitate the comparison of our results with conventional confocal and two-photon scanning microscopy. We further define

$$\bar{z}^* \equiv \frac{f_O}{f_D} \cdot \frac{\pi\, \tau_0\, C_0\, \mathrm{NA}}{n\,\lambda} = \frac{\pi\, \tau_0\, C_0}{\lambda\, \alpha\, f_D} \cdot \frac{f_O\, \mathrm{NA}}{n}, \tag{8}$$

whereby at $\bar{z} = \bar{z}^*$, $\tau_{\mathrm{eff}} \approx 2\tau_0$, i.e., $z = z_R \bar{z}^*$ indicates positions at which the effective pulse width is doubled. For two-photon excitation, this corresponds to the positions where the fluorescence signal drops to half of the maximum. In conventional confocal and two-photon scanning microscopy, the corresponding $\bar{z}^* \approx 1$. From the calculations outlined in Fig. 3, we find that optical sectioning is comparable with conventional confocal microscopy, with either moderate (0.3–0.75) or high (>1) NA objectives. Moreover, we find that laser pulses of 100-fs pulse width are sufficient to provide such sectioning effects.

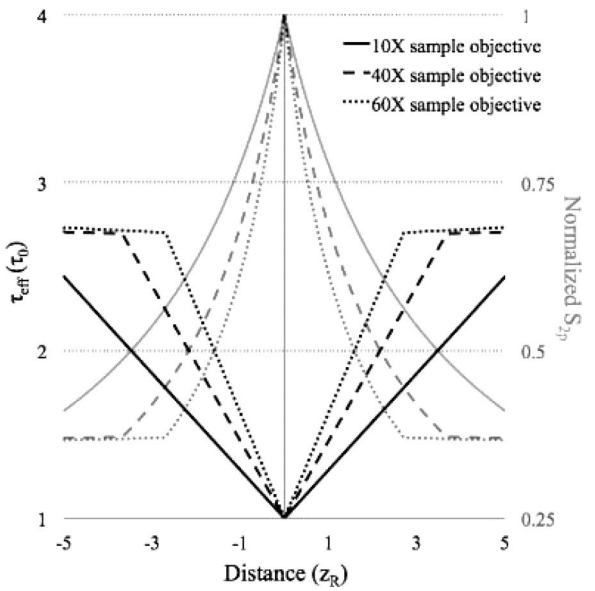

Fig. 3 Effective pulse width and two-photon excitation strength as a function of z under different sample objectives. The numerical results were obtained from Eq. (6). Notice that Eq. (8) predicts $\bar{z}^* \approx 3.53$, 2.21, and 1.62 for these objectives, respectively, which are comparable with the numerical results. To estimate the normalized strength of two-photon excitation S_{2p}, the pulse energy was set as a constant and the inverse of τ_{eff} was used to represent S_{2p} [Eq. (12)]. The horizontal (distance) and vertical (τ_{eff}) axes are expressed in units of Rayleigh length and τ_0, respectively. Parameters: $f_D = 160$ mm, $D = 100\,\mu$m, $\alpha = 1$, $d = 200$ mm, $\lambda = 800$ nm, and $\tau_0 = 100$ fs. Sample objective 10×: NA = 0.3, $f_O = 16$ mm, $n = 1$. Sample objective 40×: NA = 0.75, $f_O = 4$ mm, $n = 1$. Sample objective 60×: NA = 1.1, $f_O = 2.67$ mm, $n = 1.33$ (water immersion).

2.2 *Efficiency of Multiphoton Excitation at Low Repetition Rate*

To solve the limitation of low frame rate, we next examine how the repetition rates of pulsed lasers influence the efficiency of two-photon excitation (at constant average power). In short, we find that a 10^5-fold increase in signal-to-noise ratio (SNR) is obtained by lowering the repetition rate from 100 MHz to 1 kHz, thus providing a signal level comparable to that of conventional multiphoton and epifluorescence microscopy.

For simplicity, we consider a two-photon excitation process and estimate the light intensity required for wide-field two-photon excitation. The fluorescence signal obtained from a single laser pulse at a single pixel is

$$s_{2p} = \beta \cdot I_p^2 \cdot \tau, \tag{9}$$

where β is the two-photon excitation coefficient, I_p is the peak intensity of the excitation pulse, and τ is pulse width. Within a time unit, the fluorescence signal from each pixel collected at the detector (i.e., the CCD camera), S_{2p}, depends on the repetition rate of the pulsed laser f as

$$S_{2p} = s_{2p} \cdot f. \tag{10}$$

On the other hand, within a time unit, the average intensity of the pulsed laser on a single pixel is

$$I_{\mathrm{avg}} = \tau \cdot I_p \cdot f. \tag{11}$$

Here we have assumed that the intensity profile of the pulse is rectangular in the time domain. Combining Eqs. (9)–(11), we have

$$S_{2p} = \beta \cdot \frac{I_{\mathrm{avg}}^2}{f \cdot \tau} \propto \frac{1}{f}, \tag{12}$$

which suggests that for a fixed average intensity I_{avg}, the signal level can be significantly enhanced by reducing the repetition rate f. For example, lowering f from 100 MHz to 1 kHz can increase the signal 10^5-fold without increasing the average light intensity delivered to the sample. It should be noted that the I_p of our low-repetition-rate setup is of similar order of magnitude as that used in high-repetition-rate point-scanning microscopies. Thus, the signal levels of these two schemes are predicted to be comparable.

3 Methods and Materials

The light sources we used in this work are ultrafast chirped pulse Ti:sapphire amplifiers. Two different models were used for the travel convenience of the authors. Live-cell imaging was studied (see Figs. 5 and 6 and Video 1) with a Spectra-Physics® Spitfire® Pro, seeded with a Spectra-Physics® Mai Tai® SP ultrafast oscillator situated parallel to the amplifier within an enclosure. Quantitative characterizations of our technique (see Figs. 4, 7, 8, and 9) were carried out with a Coherent® Legend

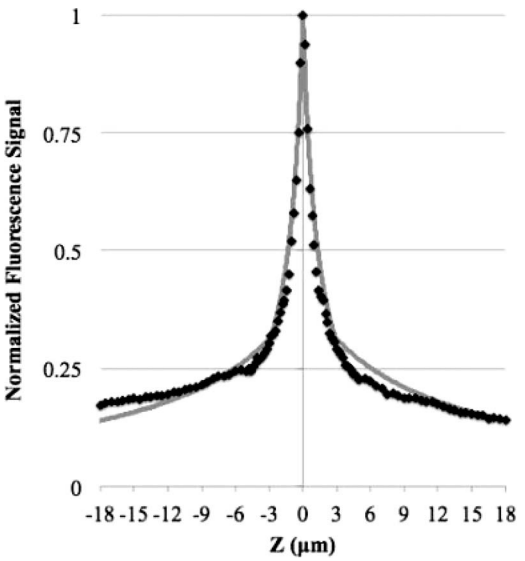

Fig. 4 Theoretical (gray line) and measured (black dots) fluorescence signal from a homogeneous dye film. The axial resolution was defined as the FWHM of the fluorescence profile. The fluorescence profile was obtained by taking optical sections of a homogeneous dye film (thickness less than 2 μm). The signal was determined by the integrating the intensity of each section. The profile was normalized by its maximum. The FWHM here is $\sim$2 μm, while the theoretical axial resolution of a confocal microscope with the same objective is $\sim$0.6 μm. Parameters in theoretical estimation and experiment: $M_{L_O} = 60$, NA $= 1.42$, $n = 1.5$ (oil immersion), $f_O = 160/60$ mm, $f_D = 160$ mm, $\tau_0 = 35$ fs, $d = 200$ mm, $\lambda = 800$ nm, $\alpha = 0.1$, $D = 30\mu$m.

Elite-USP-1k-HE, seeded with a Coherent® Mantis-5 ultrafast oscillator located parallel to the amplifier. The full width at half maximum (FWHM) pulse duration of both amplifiers was approximately 35 fs or less. The wavelength of both amplifiers was centered approximately at 800 nm with FWHM $\approx$30 nm. We expanded the beam size by a lens pair, such that the beam profile on the diffuser was two-dimensional (2D) Gaussian with FWHM $\approx$ 10 mm. The maximal output of the laser amplifier was $\sim$3 W (average power), and was attenuated to avoid thermal damage to biological samples. The average laser powers reported in Secs. 4 and 5 were all measured at the back aperture of the microscope objective L_O.

The optical diffuser employed was a Thor Labs model DG10-120. Diffusers, in general, can cause significant inhomogeneities of the light intensity at the image plane. To reduce these inhomogeneities, glass etching cream (Armour Etch®) was used to etch the diffuser. The roughness parameters D and α of the diffuser were found to be 30 μm and 0.1 after etching, according to the surface profile we measured (data not shown).

As shown in Fig. 1, the collimated laser beam is scattered by the optical diffuser, collected by the diffuser lens L_D, and then projected to the sample via the sample objectives (LUMFLN 60×W NA 1.1, PLANAPO N 60×O NA 1.42, and UPLFLN 10×NA 0.3, Olympus). The LUMFLN model objective was used for the living biological samples owing to its long working distance. The PLANAPO objective was used for the quantitative characterizations and the fixed biological sample. The UPLFLN objective was used for demonstration of large fields of view. Because our theoretical model is based on geometrical optics, it is essential that L_D has sufficient NA to geometrically resolve the scattering structures. In practice, L_D with $f_D = 160$ mm and NA $\sim$0.2 was chosen.

The chromatic dispersion of the full optical path was precompensated by the built-in compressor of the ultrafast amplifier(s) such that the signal level at the IP was optimized. The image was obtained by a CCD camera (iXon DU-885K, Andor) through L_I. The field of view is square and of length $\sim$ 6.4 mm/M_{L_O} per side, where M_{L_O} is the nominal magnification of L_O. The illumination field is 2D Gaussian with FWHM $\approx$ 10 mm/M_{L_O}. A larger illumination field or more uniform profile can be obtained by further expanding the laser beam before the optical diffuser.

The axial resolution was determined by taking images along the optical axis of a homogeneous film (thickness less than 2 μm) of fluorescent dye (F-1300, Invitrogen). For live cell imaging, we used human mammary gland MCF-10A cells expressing cyan fluorescent protein-conjugated histone (H2B-cerulean), which binds to chromosomes and has been widely used to indicate cell nuclei. MCF-10A cells were seeded in 3D matrigel (BD Matrigel™) for 10 days to form bowl-shape cell clusters several hundred micrometers in size. We then used the cell clusters to evaluate the high-frame-rate acquisition and optical sectioning capabilities of our PPMP microscope. Following the acquisition of optical sections, 3D views of the epithelial tissue were reconstructed using the ImageJ 3D Viewer.

To compare the imaging speed of our setup with that achieved by a temporal focusing microscope using a nonamplified oscillator,[9] we imaged dye-stained Mardin Darby canine kidney (MDCK) cells. The cells were cultured on glass for 2 days, followed by fixation with 4% paraformaldehyde and staining with Hoechst 33342 (a chromosome-staining dye from Invitrogen, comparable in brightness to the DAPI dye used in Ref. 9).

4 Results

4.1 *Axial Resolution of Plane-Projection Multiphoton Microscopy is Comparable to Conventional Confocal Microscopy*

Figure 4 shows the axial resolution of the optical setup depicted in Fig. 1. The axial resolution was determined by the FWHM of the fluorescence signal. With $M_{L_O} = 60$, NA $= 1.4$, $n = 1.5$, the axial resolution was found to be $\sim$2 μm, and the corresponding $\overline{z}^* \approx 3$. This is comparable to the axial resolution of an optimized conventional confocal microscope, which has $\overline{z}^* \approx 1$. Note that it should be possible to obtain an axial resolution of $\overline{z}^* \approx 1$ by optimizing the microscope design, as we described in Sec. 5.

4.2 *Frame Rate of Plane-Projection Multiphoton Microscopy is Comparable to Conventional Epifluorescence Microscopy for Live-Tissue Imaging*

To demonstrate that PPMP microscopy has the capability of imaging live tissues at high frame rate, we performed optical sectioning of live, three-dimensional MCF-10A cell clusters having hemispherical shapes (Fig. 5). The images were then used to reconstruct the 3D view (Fig. 6 and Video 1). Here, the exposure time was set at 200 ms, equivalent to 5 fps, which is

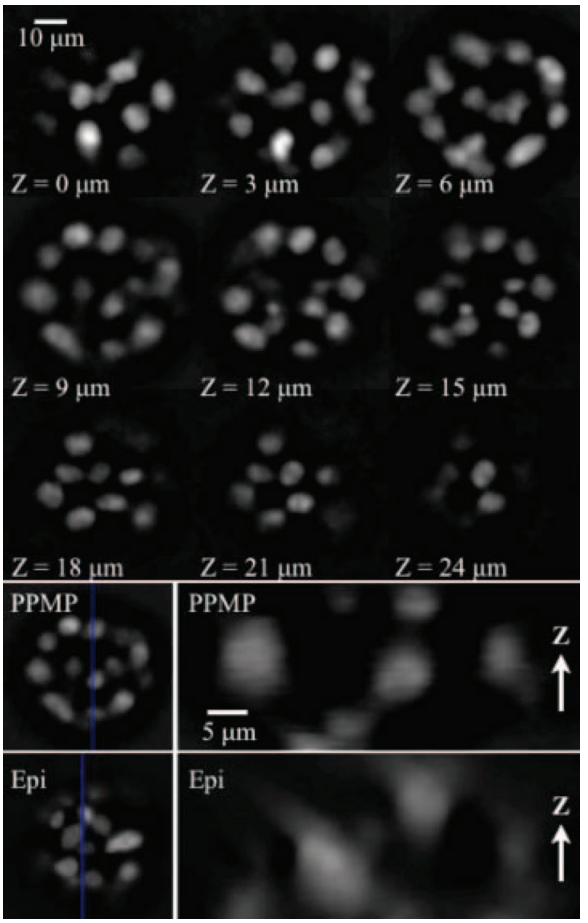

Fig. 5 Optical sections and lateral view of live MCF-10A cells in a hemispherical structure. The top panel shows the sections at different depths. The middle and bottom panels show the reconstructed lateral views under a PPMP microscope and an epifluorescence microscope (Epi), respectively. In the lateral view from the epifluorescence microscope, we clearly observe the residual out-of-focus light at the top and bottom edges of the nuclei. The lines in the middle of the top views indicate the positions where the lateral views were taken. Fluorescence signals were from cell nuclei expressing cyan fluorescent protein-conjugated histone (H2B-cerulean), which binds to chromosomes. Exposure time of each frame: 0.2 s. L_O: 60×, NA = 1.1, n = 1.33. Step size: 1 μm. Laser average power: <10 mW.

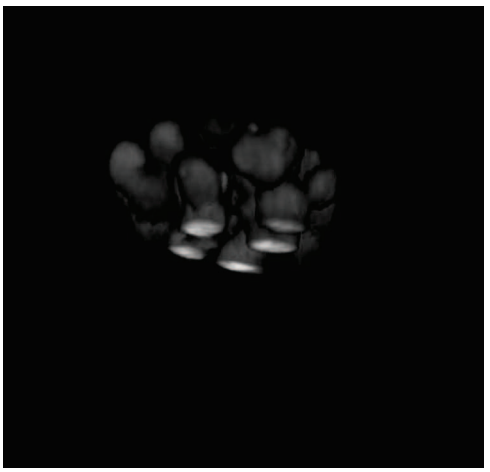

Video 1 Reconstructed 3D view of the live MCF-10A cells in Fig. 5. The 3D view was reconstructed from 40 sections with a 1-μm step size, using ImageJ 3D Viewer (QuickTime, 2.1 MB).
[URL: http://dx.doi.org/10.1117/1.3647570.1]

10 times faster than the conventional multiphoton microscope we also used to image the same sample, and is 150 times faster than a temporal focusing setup using a nonamplified 75-MHz Ti:sapphire oscillator to image cells stained with (much brighter) fluorescent dye.[9] Such an exposure time also lies within the same order of magnitude of that typically used in conventional epifluorescence microscopy (100 ms), which we also used to image the same sample (Fig. 5, lower panel) through the same CCD camera with a mercury vapor lamp (X-Cite® 120Q, Lumen Dynamics, attenuated by OD 2 to prevent significant photobleaching). Figure 5 demonstrates resolution of the boundaries of cell nuclei along the z axis (i.e., the optical axis). Nuclei in the PPMP image appear oval in structure, resembling the normal shape of cell nuclei. In contrast, the lateral view obtained from epifluorescence microscopy (Fig. 5, lower panel) shows distortion of the proper cell nuclear shape, due to the spreading of the out-of-focus signal in an epifluorescence microscope. These results suggest that PPMP microscopy can obtain high-frame-rate optical sectioning on live tissues.

4.3 *Inhomogeneity of the Illumination Field Can be Reduced by Rotating the Diffuser*

In this study, we found that conventional diffusers can cause a significant inhomogeneity of the light intensity in the illumination field, i.e., bright spots [Fig. 7(a)]. Although optical diffusers are known for generating speckle when used with temporally and spatially coherent light sources,[10] we believe that the observed field inhomogeneity is not from speckles, but rather is an effect of the diffuser used.

One way to examine the physical basis of the field inhomogeneity is to compare the images of a (homogeneous) fluorescent film with the diffuser at the focus and at a position slightly out of focus (i.e., with the diffuser translated along the optical axis by a short distance). If the bright spots are speckles, slightly defocusing the diffuser will only rearrange the location of the speckles, while the statistical properties such as the mean and the variation of brightness will remain the same.[10] The results of this experiment are shown in Fig. 7. After the diffuser was translated ~3 mm from its in-focus position, the bright spots appearing in the in-focus image [Fig. 7(a)] were found to remain in place and become dimmer and blurred [Fig. 7(b)]. These measurements suggest that the observed bright spots are not from the speckle effect, but rather from the randomness of the scattering structures distributed on the diffuser surface.

The observed field inhomogeneity also leads to inhomogeneous sectioning across the field of view; the level of which can be measured by imaging a homogeneous dye film, then separating the field of view into several areas and comparing the FWHMs of their intensity profiles. In our setup, the standard deviation of the FWHMs was found to be ~0.3 μm. One way to reduce this inhomogeneity is through the use of multiple diffusers. However, each diffuser would generate a certain level of time delay and thus contribute to pulse broadening. At the image plane, the telescoping can only recover the pulse width at the

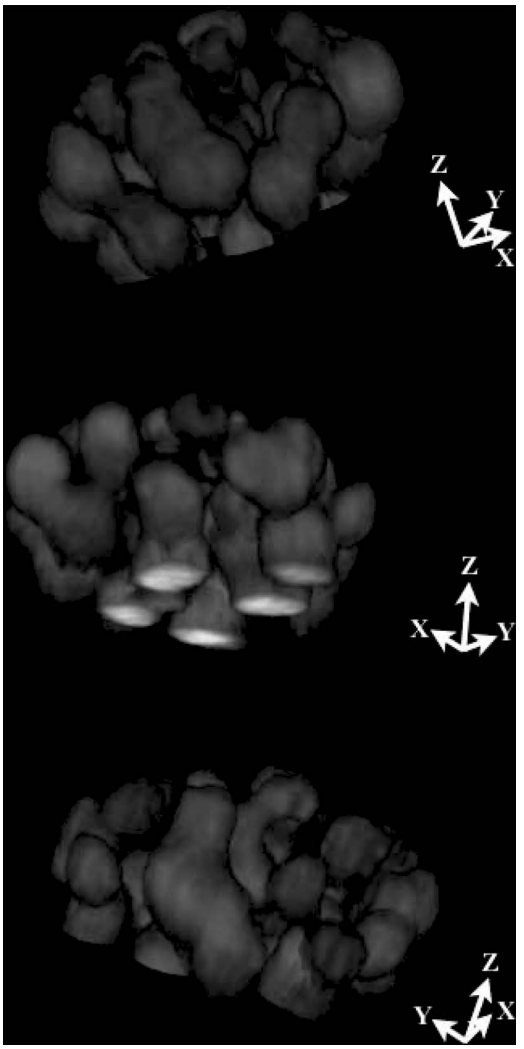

Fig. 6 Reconstructed 3D view of the live MCF-10A cells in Fig. 5. The 3D view was reconstructed from 40 sections with a 1-μm step size using ImageJ 3-D Viewer. Note that the boundaries of cell nuclei along the z axis (i.e., the optical axis) can be clearly observed; a capability that cannot be achieved by conventional epifluorescence microscopy.

input to the last diffuser (after it has already been broadened by the first diffuser). Thus, having multiple tandem diffusers can reduce the axial resolution of the optical sectioning. One way to mitigate this effect is by proper ordering of the diffusers. As mentioned in Sec. 2, diffusers with larger D and α induce longer random time delay. Therefore, in such multiple-diffuser setups, the diffuser with smaller D and α should be placed before the one with larger D and α. As an alternative solution, we have chosen to simply rotate the diffuser. By rotating the optical diffuser during the acquisition of a single frame, the inhomogeneities in the illumination field are averaged out. This effect is demonstrated in Fig. 8.

5 Discussion

5.1 *Optimization and Limit of Axial Resolution*

Here we discuss the further optimization of PPMP microscopy, and the axial resolution limit that can ultimately be obtained,

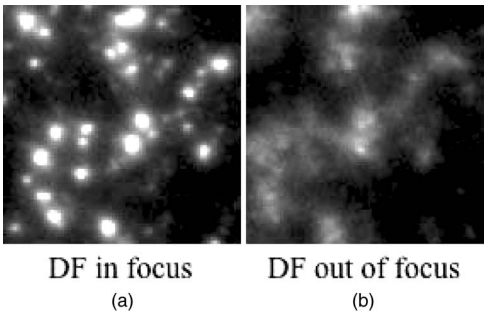

Fig. 7 Images of illumination field inhomogeneity with the optical diffuser (a) in-focus and (b) out-of-focus. For the out-of-focus image, the optical diffuser was translated for ~3 mm along the optical axis from the in-focus position. Here we can see that the out-of-focus image does not possess the same magnitude of field inhomogeneity as the in-focus image. However, while blurred, the locations of the bright spots are preserved in the out-of-focus image, consistent with the field inhomogeneity resulting not from speckle, but rather from the randomness of the scattering structures on the surface of the diffuser. The sample is a homogeneous dye film. The dimension of the field shown here is 70 × 70 pixels.

as derived within the realm of geometrical optics. Equation (8) suggests that $\overline{z}^*$ can be further reduced by using an objective with a higher magnification and NA (which often exhibits a smaller $f_O\,NA/n$), as shown in Fig. 3. Likewise, increasing f_D, α, or reducing τ_0 leads to smaller $\overline{z}^*$. We stress that these estimations are derived based on geometrical optics, and so may not be valid in the extreme case where $\overline{z}^* < 1$, in which case the optimal axial resolution of our temporal focusing setup would be the same as that of a laser scanning microscope.[9]

A further fundamental advantage of diffuser-based temporal focusing over blazed grating approaches is that the diffuser-based technique can achieve the axial resolution of a point-scan setup, whereas (single) grating-based temporal focusing is limited to that of a line-scan setup. The difference arises from the way in which the time delays are generated. For optical diffusers, the time delay results from the surface roughness of the diffusers, which creates a 2D spatial profile for the randomness of the time delay. In contrast, the time delay in grating-based temporal focusing is created by the one-dimensional scan of the laser pulses on the grating surface; such a mechanism restricts the time

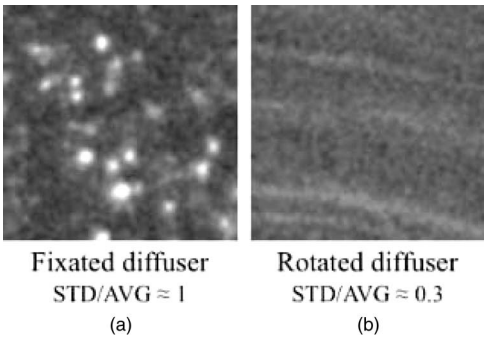

Fig. 8 Illumination field intensity inhomogeneity with (a) fixed and (b) rotated optical diffusers. The field inhomogeneity is defined as the standard deviation of the field divided by the average intensity of the field. The field inhomogeneity is greatly reduced by rotating the optical diffuser during the exposure of each frame. The sample is a homogeneous dye film. The dimension of the field shown here is 100×100 pixels.

delay to be one-dimensional. This restriction has been overcome by using two orthogonally aligned gratings.[11] In such a setup, the two gratings must differ in groove density sufficiently, such that the scanning of the laser pulse can be well separated in two orthogonal dimensions. Such a design increases the complexity of the apparatus and will likely require multiple pairs of gratings when multiple/tunable excitation wavelengths are used.

From Eq. (4), the spread, or distribution, of arrival times produced from the surface roughness of a diffuser is upper bounded by the factor D. This suggests that diffusers with larger D should be used to ensure a sufficiently large spread of arrival times. The roughness of the diffuser surface, however, leads in turn to roughness of the image plane, D'. Using the thin lens formula, we estimate D' to be $(f_O/f_D)^2 D$. This suggests that D' can be negligible if $f_D \gg f_O$. Thus, with a proper arrangement of parameters, the roughness of the image plane can be reduced below one Rayleigh length, while the surface roughness of the diffuser is sufficiently large to create temporal focusing.

5.2 *Limitation of Frame Rate and Benefits of Low Repetition Rate*

For live-tissue imaging, the frame rates of our setup are limited by the low SNR of fluorescent proteins expressed in living systems. Nevertheless, Eq. (12) suggests that SNR can be further enhanced by lowering the repetition rate while maintaining the average power of the laser. For example, the frame rate of our setup can be further increased by equipping our system with a pulsed laser of much lower repetition rate, e.g., 100 Hz. With such a low repetition rate, Eq. (12) suggests a 10-fold stronger SNR than what is presented in this study. This would lead to a frame rate of up to 50 fps, a rate sufficient to study most biological processes such as cell division, migration, and polarization.

This limiting frame rate is estimated for imaging the fluorescent proteins expressed in living systems. This limitation is relaxed, though, if the signals are derived from materials with strong fluorescence efficiency such as fluorescent dyes and nanoparticles. In such cases, we are able to achieve higher frame rates, as shown in the top panel of Fig. 9, which was obtained with an imaging speed 1000 times faster than a temporal focusing setup using a nonamplified 75 MHz Ti:sapphire oscillator and a similarly dyed sample.[9] Furthermore, by using microscope objectives of low magnification, we can also achieve large fields of view. This capability for large field of view is demonstrated in the bottom panel of Fig. 9, where we imaged dye-stained MDCK cells with a 10× objective. The size of the field of view shown here is 0.6 × 0.6 mm^2 and the exposure time was 100 ms.

Our setup can achieve these larger fields of view with a relatively short exposure duration simply because the 1-kHz amplifier is very powerful; that is, because it is supplying its average power at a low repetition rate and low duty cycle and thus achieving a high peak power. To generate multiphoton excitation at the level required for imaging with reasonable frame rates, the peak intensity is commonly around or greater than 1 kW/μm^2.[12] Therefore, to excite an area up to 1 mm^2, one needs a light source with peak power greater than 10^9 W. The maximal peak power of our amplifier is roughly 10^{11} W, and is thus powerful enough to support a large field of view for most microscopy applications. It should be noted that in the original temporal focusing setup,[9]

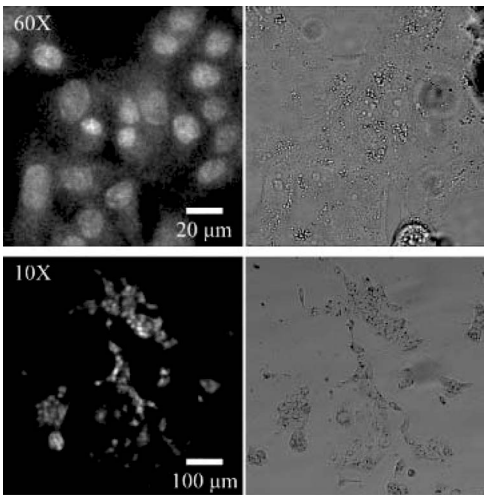

Fig. 9 MDCK cells stained with fluorescent dye (left) and under bright-field illumination (right) using 60× (top) and 10× (bottom) microscope objectives. The imaging speed using the 60× objective is 1000 times faster than a temporal focusing setup using a non-amplified 75 MHz Ti:sapphire oscillator and similarly dye-stained sample (Ref. 9). Signal from areas outside of the nuclei results from non–specific staining. Exposure time: 0.03 (60×) and 0.1 (10×) seconds. L_O: 60×/10×, NA = 1.42/0.3, n = 1.5/1. Laser average power: <15/60 mW.

a 140 × 140–μm^2 field of view was obtained with an average power of 30 mW and an exposure time of 30 s. This indicates that a 1-mm^2 field of view can be achieved with that instrument by using a low magnification objective and an average power of around 1.5 W, though the exposure time in such a setup could be slightly longer than 30 s because lower magnification objectives are typically less efficient in collecting light.

However, from a biologist's point of view, we would also like to point out that discussing the imaging speed for fixed biological samples stained with fluorescent dye is less important than the speed achievable for living systems. Once a sample is fixed, using an imaging time of either 3 h or 10 s would most likely provide the same level of details and information. On the other hand, for studies of dynamic biological processes, the imaging speed would determine the temporal resolution of the observations. To the best of our knowledge, this is the first report of imaging live cells expressing fluorescent protein by a temporal focusing microscope at a frame rate faster than 1 fps.

In addition to the enhancement of the signal level and frame rate, there are certain potential benefits provided by lowering the repetition rate from the megahertz to kilohertz regime. It has been reported that the use of low repetition rates (at the same optical power) can reduce photobleaching.[13,14] This is achieved through the avoidance of dark state conversion. Indeed, a 5- to 25-fold enhancement of total fluorescence yield, before detrimental effects from photobleaching, has been reported.[13] Moreover, lowering the repetition rate is equivalent to providing the system a longer window of no excitation. This would allow slow processes such as heat dissipation to occur more efficiently, thus minimizing sample damage caused by a continuous accumulation of heat.[4] As a result, even with a similar amount of thermal energy introduced by the excitation process, a sample excited at a lower repetition rate is less likely to be damaged by heat accumulation as compared to the use of a higher repetition rate.

5.3 *Potential Applications as Structured Light Microscopy*

In principle, the inhomogeneity of the illumination field can be utilized for structured light microscopy.[6] This could be particularly useful in applications where reasonable optical sectioning, as provided by temporal focusing, is not achievable. Examples include coherent anti-Stokes Raman scattering (CARS) and stimulated Raman scattering microscopy, where picosecond pulses are generally required to obtain chemical specificity.[15,16] Based on Eq. (8), pulse widths of picosecond duration would greatly reduce the sectioning effect. Nevertheless, by using the inhomogeneity of the illumination field as a structured light source, it is possible to regain the optical sectioning of these systems, as demonstrated in a previous study.[6] This allows one to integrate CARS with multiphoton excitation in a wide-field microscope simply by using an optical diffuser.

6 Conclusion

The question of how to increase image acquisition rate and axial resolution, while maintaining a biocompatible laser dosage, is a long-standing challenge in the optical microscopy community. In this report, we have demonstrated a microscope design for live-tissue imaging that provides an axial resolution comparable to confocal microscopy and a frame rate similar to that of epifluorescence microscopy.

By utilizing an optical diffuser, a temporal focusing setup is realized with a design as simple as a conventional epifluorescence microscope. Even at a high frame rate, the photobleaching and thermal damage of PPMP microscopy could be lower than conventional multiphoton and confocal laser scanning microscopy. Compared with temporal focusing techniques using Megahertz repetition-rate laser pulse trains, the use of low repetition-rate pulses, while maintaining the same average power, can significantly enhance the SNR. In addition, using an optical diffuser instead of a blazed diffraction grating provides flexibility for multi- or tunable-wavelength light sources, and thus creates a platform for multispectral imaging and pump-probe microscopy. Taken together, these features suggest that plane-projection multiphoton microscopy can be used to study fast, three-dimensional processes in living cells and tissues, and to do so with minimal phototoxicity and thermal damage.

Acknowledgments

This work is a collaborative research effort of the Cell Polarity Laboratory at the California Institute of Technology and the Technology and Applications Center at Newport Corporation. The authors would like to thank Mr. Craig Goldberg of Newport Corporation for facilitating the collaboration, and Professor Shi-Wei Chu for the inspiring discussions. Mr. Ji Hun Kim of Caltech is sincerely acknowledged for the measurement of the surface profile of the optical diffuser. CLG recognizes support from the Ellison Medical Foundation and the Weston Havens Foundation. Support from the National Science Foundation Chemistry Research Instrumentation and Facilities: Instrument Development program to GAB is gratefully acknowledged.

References

1. J. B. Pawley, *Handbook of Biological Confocal Microscopy*, 3rd. Ed., Springer, New York (2006).
2. S. Potter, "Vital imaging: Two photons are better than one," *Current Biology* **6**(12), 1595–1598 (1996).
3. M. Cahalan, I. Parker, S. Wei, and M. Miller, "Two-photon tissue imaging: Seeing the immune system in a fresh light," *Nat. Rev. Immun.* **2**(11), 872–880 (2002).
4. B. Masters, P. So, C. Buehler, N. Barry, J. Sutin, W. Mantulin, and E. Gratton, "Mitigating thermal mechanical damage potential during two-photon dermal imaging," *J. Biomedical Opt.* **9**(6), 1265–1270 (2004).
5. J. Huisken, J. Swoger, F. Del Bene, J. Wittbrodt, and E. Stelzer, "Optical sectioning deep inside live embryos by selective plane illumination microscopy," *Science* **305**(5686), 1007–1009 (2004).
6. M. Neil, R. Juskaitis, and T. Wilson, "Method of obtaining optical sectioning by using structured light in a conventional microscope," *Opt. Lett.* **22**(24), 1905–1907 (1997).
7. A. Egner and S. Hell, "Time multiplexing and parallelization in multifocal multiphoton microscopy," *J. Opt. Soci. Am. A* **17**(7), 1192–1201 (2000).
8. T. Nielsen, M. Frick, D. Hellweg, and P. Andresen, "High efficiency beam splitter for multifocal multiphoton microscopy," *J. Micros.* **201**, 368–376 (2001).
9. D. Oron, E. Tal, and Y. Silberberg, "Scanningless depth-resolved microscopy," *Opt. Express* **13**(5), 1468–76 (2005).
10. J. W. Goodman, *Statistical Optics*, Wiley, New York (1985).
11. A. Vaziri and C. V. Shank, "Ultrafast widefield optical sectioning microscopy by multifocal temporal focusing," *Opt. Express* **18**(19), 19645–19655 (2010).
12. W. Denk, J. Strickler, and W. Webb, "2-Photon laser scanning fluorescence microscopy," *Science* **248**(4951), 73–76 (1990).
13. G. Donnert, C. Eggeling, and S. W. Hell, "Major signal increase in fluorescence microscopy through dark-state relaxation," *Nat. Methods* **4**(1), 81–86 (2007).
14. J. Mertz, "Molecular photodynamics involved in multi-photon excitation fluorescence microscopy," *Eur. Phys. J. D* **3**(1), 53–66 (1998).
15. M. Duncan, J. Reintjes, and T. Manuccia, "Scanning coherent anti-stokes Raman microscope," *Opt. Letters* **7**(8), 350–352 (1982).
16. C. Freudiger, W. Min, B. Saar, S. Lu, G. Holtom, C. He, J. Tsai, J. Kang, and X. Xie, "Label-free biomedical imaging with high sensitivity by stimulated Raman scattering microscopy," *Science* **322**(5909), 1857–1861 (2008).